Journal of Advanced Marine Engineering and Technology, Vol. 49, No. 4, pp. 283~291, 2025
J. Advanced Marine Engineering and Technology (JAMET)
https://doi.org/10.5916/jamet.2025.49.4.283

ISSN 2234-7925 (Print)
ISSN 2765-4796 (Online)
Original Paper

Autonomous tracking of a drone in open fields

Dong-Jin Kim[1] · Kyoung-Sun Jang[2] · Chan-Gu Park[3] · Sang-Do Lee[†]

(Received April 24, 2025 ; Revised June 11, 2025 ; Accepted August 22, 2025)

Abstract: Drones are widely used in marine sectors to deliver relief supplies, detect fish in fishing vessels, inspect wind turbine blades, observe large creatures on the coast, and conduct search and rescue activities. Portable drones should not be too weak or too small to operate effectively in ocean environments because of harsh weather conditions. This study investigates the autonomous tracking of a hexacopter in an open field. We check the attitudes, altitudes, communications, hovering, vibrations, and other factors. The test was conducted in the field at OSAN University on 23 January 2025. A Tarot S550 hexacopter model was prepared for autonomous tracking without joystick control. This is a basic robotics experiment. The purpose of control is achieved through an open-source program called ArduPilot. We illustrate the concepts of guidance law, control basis, and recursive estimators. The drone performed well in the tracking, driving, vibration, and hovering tests. For example, the vibrations in the X-, Y-, and Z-axes directions were less than 30 m/s/s, particularly those in the X- and Y-axes, which were less than 10 m/s/s. Three altitudes (barometer, EKF, and reference) are matched during the ascent and descent actions.

Keywords: Autonomous tracking, Drone, UAVs, ArduPilot, Maritime environments

1. Introduction

The drone industry has grown worldwide. Drones are popular among researchers and the public because they are easy to handle and are advantageous for various applications. For example, mail parcel services for recipients and shore-to-ship deliveries, which are already in operation in the UK, explain the benefits of time, cost, and emissions **[1][2]**. Drones can minimize the risk of the sea surface. Drones can complement existing mail services to rural inter-islands in the most remote places in the UK **[2]**. The maritime environment of South Korea resembles that of the UK, and the application of drones enables operation in hard-to-reach locations. Although there are many rural islands in Jeonnam Provision, the cost of transportation for a few residents should be considered.

Recently, in the US, trials of shore-to-ship operations demonstrated the application of drones in the marine industry **[3]**. Regular ships can be supplemented with drones for small requirements. Drones are widely used in marine fields to deliver relief supplies **[4]**, detect fish in fishing vessels, inspect the blades of wind turbines **[5]**, observe large creatures on the coast, and conduct search/rescue activities **[6][7]**.

In Australia, it took less than two minutes to drop life equipment using drones, where two people were in distress at sea **[8]**. However, failures in remote operation may result in accidents due to controlled descent **[9]**. Therefore, autonomous drone technology is necessary. Unmanned Aerial Vehicles (UAVs) are useful in observing and detecting maritime environments such as polar areas **[10]**.

The advantage of drones is that the preparation time for launch is short, and the initial actions are more suitable. The location of marine accidents, quick delivery, and fast reactions determine the success of missions in initial countermeasures. Therefore, the Coast Guard is investing in drones for search and rescue activities in maritime environments.

Drones are vulnerable to wind. It can fly freely in calm weather, but a weak drone finds it difficult to overcome wind forces. Weather in ocean environments is strong, and weak bodies are not durable against wind forces. The speedbird DLV-2

† Corresponding Author (ORCID: http://orcid.org/0000-0002-7001-4761): Assistant Professor, Division of Navigation & Information System, Mokpo National Maritime University, 91, Haeyangdaehak-ro, Mokpo, Jeollanam-do, 58628, Korea, E-mail: oksangdo@mmu.ac.kr, Tel: 061-240-7257

1 Ph. D. Candidate, Division of Maritime Transport System, Mokpo National Maritime University, E-mail: ican7037@naver.com

2 Ph. D. Candidate, Division of Maritime Transport System, Mokpo National Maritime University, E-mail: ypepa123@osan.ac.kr

3 Director, Flybot, E-mail: make1978@naver.com

model in **[3]** reported that the payload and maximum wind speeds are 3.99 kg and 12.5 m/s, respectively.

We believe that the bodies and blades of drones are suitable for marine environments. When we increase the size of drones, they should be operated under other laws. Therefore, a large wing system, such as the Windracer **[11]** is beyond the scope of this study. Therefore, we selected a hexacopter, rather than a quadrotor, for our tests. Considering the wind endurance in maritime environments, we selected the Tarot S550 hexacopter model and developed an autonomous tracking system.

Le and Nam introduced hexacopter modeling and illustrated the results of motor speed and trajectory tracking based on a proportional integral derivative (PID) control design **[12]**. However, no actual tests or autonomous systems of relevance to the hexacopter can be found. The difference between this paper and previous publications is that it shows the experimental results of an autonomous tracking test based on the PID control scheme of a hexacopter.

We created the drone ourselves. All materials for the autonomous tests were supplemented by the Flybot Company in Seoul. The tracking problem was solved using the ArduPilot open-source program **[13]**. This is a basic drone experiment in robotics. We briefly introduce the ArudPilot control system, in which the concepts of the extended Kalman filter (EKF) and guidance law are essential for UAVs.

Very recently, some studies have demonstrated the use of ArduPilot and Mission Planner (MP) applications for UAVs **[14-16]**. However, the hovering results of their tests were not observed in their experiments. A literature review of UAV systems has been reported **[17]**, and the concept of the Kalman filter is widely used in the control community **[18]**. In this paper, to complement the basic knowledge of observer-based control, we present a simple paragraph that is structured around our experimental research rather than a numerical simulation.

Section 2 explains the theoretical background and experimental setup. Section 3 presents the results of autonomous tracking. The conclusion is given in Section 4.

2. Theoretical Background

2.1 Basic Frames of a Drone

The basic framework of the drone is discussed in this section. The two drone frames are illustrated in **Figure 1**. However, for simplicity, the North-East-Down (NED) frame was not included in this study. The blue coordinate is an earth-fixed frame ($X_E Y_E Z_E$, subscript means 'earth'), and the red coordinate is a body-fixed frame ($o_b x_b y_b z_b$, subscript means 'body'), whose center of gravity (o_b) is fixed on the drone. According to the right-handed rule, the right thumb indicates the positive direction and the other four fingers curl in the direction of rotation.

The Euler angles ϕ, θ and ψ denote the roll, pitch, yaw, and their time derivatives p, q and r indicate their angular velocities (rates) concerning the axes $x_b y_b z_b$. The position in three-dimensional space is dependent on the angles of $\phi$and the total forces of rotors. When we want to move forward in the x_b direction, the head of a drone should be bent to make the rotational angles of pitchθ.

Following the ArduPilot document **[19]**, the motor direction and number of hexacopters were set, as shown in **Figure 2**. The blue direction indicates clockwise (CW) and red is CCW counterclockwise (CCW). Reaction forces occur when CW and CCW rotate. Starting from 1 and 2 in the y-axis direction, the symmetric x-bars are numbered 3, 4, 5, and 6. w_i are the angular frequencies of the motors and f_i are the lift forces, which are the control inputs of the position and rotational controllers in the numerical simulation.

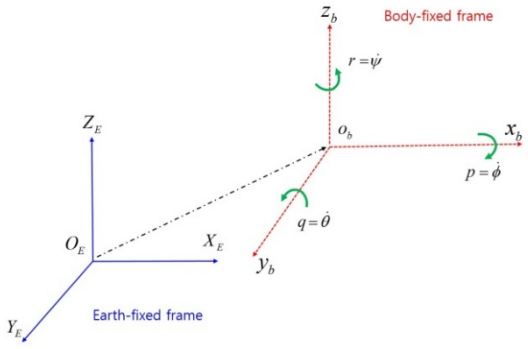

Figure 1: Basic frames of a drone

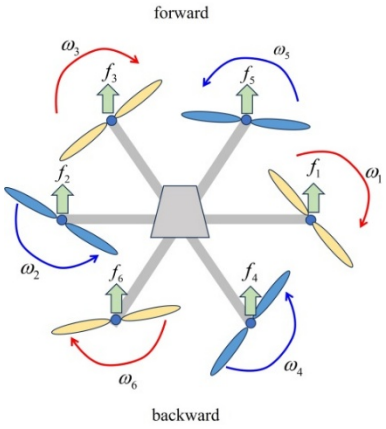

Figure 2: Hexacopter motor direction

Based on **Figures 1** and **2**, the rotation matrix is given as

$$R = \begin{bmatrix} C_\psi C_\theta & C_\psi S_\theta S_\phi - S_\psi C_\phi & C_\psi S_\theta C_\phi + S_\psi S_\phi \\ S_\psi C_\theta & S_\psi S_\theta S_\phi + C_\psi C_\phi & S_\psi S_\theta C_\phi - C_\psi S_\phi \\ -S_\theta & C_\theta S_\phi & C_\theta C_\phi \end{bmatrix} \quad (1)$$

where $S_{(\cdot)} = sin(\cdot)$and $C_{(\cdot)} = cos(\cdot)$. Rotational kinematics can be obtained from the relationship between the rotation matrix and its derivative with a skew-symmetric matrix as follows **[20][21]**:

$$\dot{\vartheta} = W_\eta^{-1} \nu \quad (2)$$

$$\begin{bmatrix} \dot{\phi} \\ \dot{\theta} \\ \dot{\psi} \end{bmatrix} = \begin{bmatrix} 1 & S_\phi T_\theta & C_\phi T_\theta \\ 0 & C_\phi & -S_\phi \\ 0 & S_\phi SC_\theta & C_\phi SC_\theta \end{bmatrix} \begin{bmatrix} p \\ q \\ r \end{bmatrix}$$

where $T_{(\cdot)} = tan(\cdot)$, $SC_{(\cdot)} = sec(\cdot)$, $\Lambda = [\phi \quad \theta \quad \psi]'$ and $\nu = [p \quad q \quad r]'$. Because this study does not present the simulation results based on the control scheme of the hexacopter, the mathematical formulation, including the motor dynamics and control design, is omitted.

2.2 Control System and Measurement Principles

Figure 3 shows the control system of ArduPilot **[22]**. The figure is based on a diagram on the website. The control parts and plants were used. In the plant diagram, the motor mixer, the electronic speed controllers (ESCs), and hexacopter dynamics are mathematically formulated. The measurements include well-known GPS, gyroscopes, accelerometers, magnetometers, and barometric pressures **[23]**. The position and attitude controllers are based on the PID control in the ArduPilot system. This is a low-level controller. The UAV control system is connected to the inner and outer loops. For example, to move the drone forward, the pitch angle should be set as the reference. The desired acceleration is necessary to control the angle-control rate. We can imagine that the drone control system should be connected in a straight line with a boundary to escape the singularity. The inputs are continually corrupted by white noise, which is expressed as a chirp signal in the waveform. Thus, the EKF and filters are necessary in the experiment.

As shown in **Figure 3**, a Kalman filter (KF) is employed as an observer to estimate the state vector **[18]**. The KF is a state estimation algorithm implemented in stochastic control systems that generates control inputs based on unmeasurable variables. The KF is an optimal observer **[24]**, which means that this recursive filter is utilized based on knowledge of the statistical model, measurement dynamics, initial conditions, noise, and errors **[25]**.

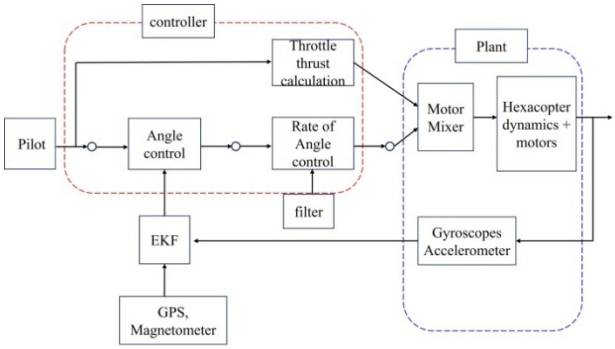

Figure 3: ArduPilot control system

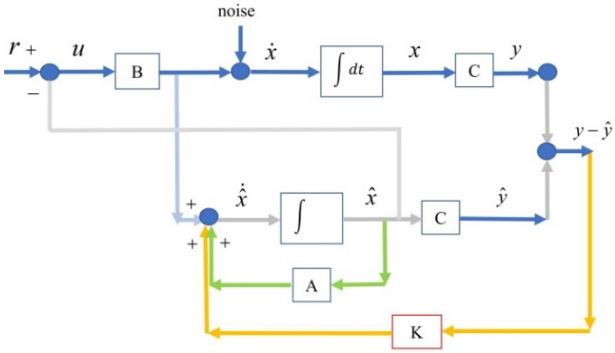

Figure 4: Tracking and observer systems

This filter advances the Gaussian concept for least-squares problems.

The EKF is an extended version for handling nonlinear measurements and unknown systems. It is used to estimate the position, orientation, and velocity of the drones. We briefly introduce the theoretical background and illustrate the observer flow in **Figure 4**. This filter can minimize errors between the measurement and actual states **[26]**.

The state-space of the control system is expressed in normal form.

$$\dot{x} = Ax + Bu$$
$$y = Cx \quad (3)$$

where x is the state vector (n vector), y is the output, A is an $n \times n$ state matrix, B is an $n \times 1$ input matrix, and C is a $1 \times n$ output matrix **[27]**. The observer equations are given as

$$\dot{\hat{x}} = A\hat{x} + Bu + K(y - \hat{y})$$
$$\hat{y} = C\hat{x} \quad (4)$$

where $\hat{x}, \hat{y}$are the estimates of $x$and y, respectively, K is the observer gain. Subtracting (4) to (3) yields

$$\dot{x} - \dot{\hat{x}} = A(x - \hat{x}) + Bu - Bu - KC(x - \hat{x}) \quad (5)$$

Setting the observer error as $x - \hat{x} = e$,

$$\dot{e} = (A - KC)e \quad (6)$$

When e approaches zero, the observer becomes asymptotically stable. The real part of the eigenvalues, the $A - KC$ matrix, is negative.

Similarly, the true state x_k and measurement z_k at time k in the KF are considered as follows:

$$\begin{aligned} x_k &= F_k x_{k-1} + B_k u_k + w_k \\ z_k &= H_k x_k + v_k \end{aligned} \quad (7)$$

where F_k is the state transition model; B_k is the control-input model; u_k is the control vector, H_k is the observation model; w_k, v_k are noises **[28]**. This filter uses the estimate and variance. Similar to (4), the predicted state estimate $\hat{x}_k$ and update $\tilde{y}_k$of the filter are expressed as follows:

$$\begin{aligned} \hat{x}_k &= F_k \hat{x}_{k-1} + B_k u_k \\ \tilde{y}_k &= z_k - H_k \hat{x}_k \end{aligned} \quad (8)$$

In the EKF, a nonlinear function is used in the state transition and observation model, as follows **[29]**:

$$\begin{aligned} x_k &= f(x_{k-1}, u_{k-1}) + w_{k-1} \\ z_k &= h(x_k) + v_k \end{aligned} \quad (9)$$

The system and measurement model can be represented as:

$$\begin{aligned} \dot{x}(t) &= f(x(t), u(t)) + w(t) \\ z_k &= h(x_k) + v_k \end{aligned} \quad (10)$$

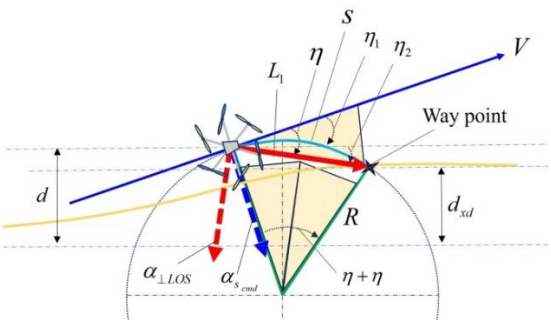

Figure 5: Guidance concept of UAV

where $x_k = x(t_k)$ **[29]**. Detailed information on the principles of the EKF can be found in literature. This study is not aimed at the EKF; further information, such as updated equations in the discrete system, error covariance, and Kalman gains, can be obtained from other studies **[30][31]** or books **[32][33]**.

2.3 Tracking Control Problem

Unlike regulation, the tracking control problem has a reference input in the block diagram of the control scheme, as shown in **Figure 4**. For tracking missions, the longitude and latitude positions were provided as reference inputs in the (MP) screen of the ArduPilot application **[34]**. A PID controller is used to achieve its tracking goal **[35]**. To fulfill the tracking purpose, the PID gains should be tuned on the MP screen **[36]**. The 'P' gain of roll is important for autonomous experiments. Tuning of PID gains can be observed on the website **[37]**.

The principles of tracking control are shown in **Figure 5**. This concept is ameliorated to guide UAVs **[38][39]**. It originates from the theory of centripetal acceleration and the control law relating to the lateral track errors of UAVs on a North-East frame **[40]**. The local position of the drone to the next target can be regarded as the so-called L1 distance (L_1). Normally, as the drones are not on the surface of the Earth, an angle (η) exists between the forward direction of velocity (V) and the direction of L_1. We assume that the angles (η_1, η_2) are small, such as $sin\,\eta \approx \eta = \eta_1 + \eta_2$. The angles of η_1 and η_2 are approximately equal to $\frac{d - d_{xd}}{L_1}$ and $\frac{\dot{d}}{V}$, respectively. Centripetal acceleration occurs when the drone moves to the next WP. The dashed lines in **Figure 5** can be defined as **[38][39]**:

$$\alpha_{\perp LOS} = 2\frac{V^2}{L_1} sin\,\eta\, cos\,\eta \quad (11)$$

$$\alpha_{s_{cmd}} = 2\frac{V^2}{L_1} sin\,\eta \approx 2\frac{V}{L_1}(\dot{d} + \frac{V}{L_1} d) \quad (12)$$

In addition, $\alpha_{s_{cmd}}$ is approximately equal to $-\ddot{d}$, the **Equation (12)** can be written as a 2nd-order Ordinary Differential Equation (ODE):

$$\ddot{d} + 2\zeta\omega_n \dot{d} + \omega_n^2 d \approx 0 \quad (13)$$

With $\zeta = \frac{k_c}{2\sqrt{m k_s}} = \frac{1}{\sqrt{2}} = 0.707$ and $\omega_n = \sqrt{\frac{k_x}{m}} = \frac{\sqrt{2}V}{L_1}$

where ζ is the small damping coefficient; ω_n is the natural frequency of a resonator; m is the mass; $k_c, k_x (> 0)$ are the

damping and restoring constants of a Mass-Damper-Spring system, respectively. From the nonhomogeneous ODE, the form of driving force can be thought of as $\frac{F_0}{m} cos\ \omega_n\ t$ **[41]**, the control input can be added in a state-space representation as follows **[33]**:

$$\begin{bmatrix}\dot{x}_1(t)\\ \dot{x}_2(t)\end{bmatrix} = \begin{bmatrix}0 & 1\\ -\omega_n^2 & -2\zeta\omega_n\end{bmatrix}\begin{bmatrix}x_1(t)\\ x_2(t)\end{bmatrix} + \begin{bmatrix}0\\ 1\end{bmatrix}u(t) \quad (14)$$

General solutions and UAV applications for AruduPilot can be found in the book and on the website. Because this case is a linear equation, one can apply similar dynamics to marine vessels for nonlinear equations with advanced control theories, such as adaptive super-twisting or fractional-order sliding mode control. However, previous studies focused on numerical simulations without the observer concept. This study addresses observer-based guidance control laws.

3. Experimental Test

3.1 Experimental Space and Waypoints

On 23 January 2025, an experimental test was conducted in the open fields of OSAN University, as shown in **Figure 6**. All members gathered at the spot. It was cold, but the wind was weak. The daily mean wind speed in OSAN City was 2.0 m/s. **Table 1** lists the waypoints (WPs) for the latitude and longitude in decimals. The takeoff point is 37°09′16.22″N, 127°03′37.8″E with DMS (degrees, minutes, seconds) style. The takeoff is green, WPs 1–9 are blue, and the finish is WP 9 in red symbols (**Figure 7**).

The autonomous tracking mission comprised orthogonal routes. The purpose of this test was to evaluate the performance of the trajectories, hovering, vibrations, differences in position information, wind resistance, communication, and battery duration. Although the weather was not strong, this result confirmed that the size of the model can be used in ocean environments. However, the battery life should always be considered when using it far from the ocean. During an emergency, a drone can be manually retrieved.

Table 1: Waypoints (WPs) on the MP screen

WPs	Latitude	Longitude
Takeoff	37.1545021	127.0605015
1	37.1547514	127.0600247
2	37.1545115	127.0597963
3	37.1542715	127.0602044
4	37.1544566	127.0603777
5	37.1546485	127.0600481
6	37.1545193	127.0599291
7	37.1543887	127.0601945
8	37.1544541	127.0602191
9	37.1545211	127.0601069

Figure 6: Hexacopter on the ground

Figure 7: Takeoff (green symbol) and finish point (red symbol)

3.2 Experimental Results

The EKF system estimates 22 states **[23]**, for example, four quaternions, three velocities, three positions in a NED frame, and three gyro biases. In this study, we had to reduce the number of results because of the lengthy content. It generates the orientation, velocity, and position. We compared the results of the EKF and Attitude and Heading Reference System (AHRS) positions (**Figure 8**). The names of the data are represented in the same manner as in MP. The outcomes of the EKF appeared clean of noise; however, there were some biased errors between the two datasets. As it is depicted in a North-East frame, the GPS result was prepared to determine the local position (**Figure 9**). The cornering of our model exhibited curved lines. Outbound tracking is not observed at the corners. Drones are effective at autonomously tracking WPs.

The attitudes (pitch, roll, and yaw) are shown in **Figures 10**-

12, respectively. The pitch and roll seldom vibrate beyond 10 °. The pitch responses became positive after 1500 s. We believe that the drone raised its head during short intervals from WPs 6–8. The negative peak value of eight times shows that the drone was tilted to the left from WPs 1–8. However, quick recovery was achieved. This feature seems unfamiliar to marine vessels because fast restoration affects the comfort of passengers or crew on board.

The drone moved regularly according to the yaw response. In **Figure 5**, the yaw angle lies between the true north and forward velocity (V). In the experiment, the drone was not significantly affected by wind forces. In future tests, we plan to prepare for bad weather on the coast of South Korea. Sometimes, the UAVs fail in their tracking courses. In the Introduction, the speed-bird DLV-2 model can endure wind speeds of 12.5 m/s; however, we cannot conclude how much our model can resist wind gusts from this experiment only.

Hovering is one of the interests of this study. The EKF is responsible for estimating altitude from the sensors. The controller considers the desired (reference) and estimated altitudes. As the three altitudes (barometer, EKF, and reference) match well, hovering demonstrates good performance in the ascent and descent actions (see **Figure 13**). Not all 'altitudes' have the same meaning **[42]**.

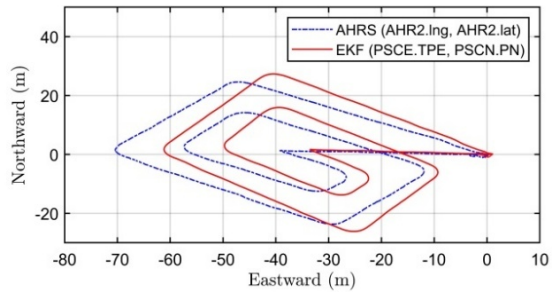

Figure 8: Results of EKF and AHRS positions

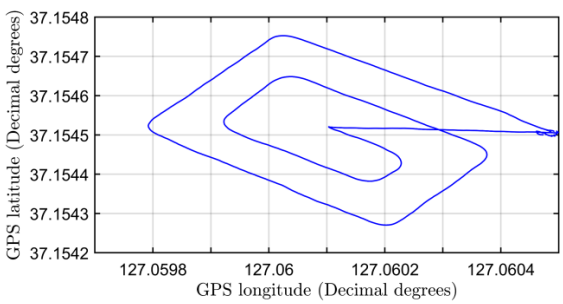

Figure 9: Results of GPS trajectories

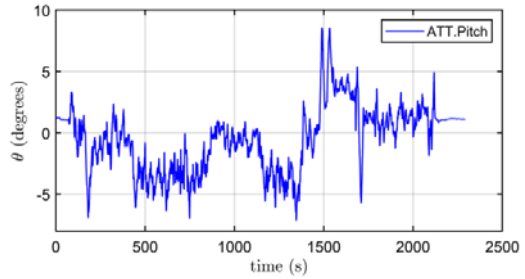

Figure 10: Pitch responses

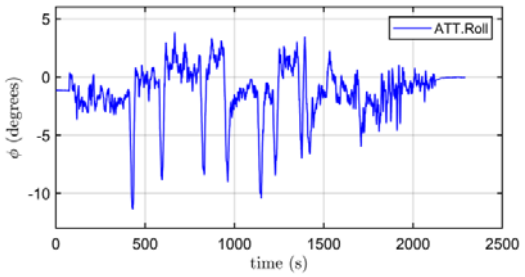

Figure 11: Roll responses

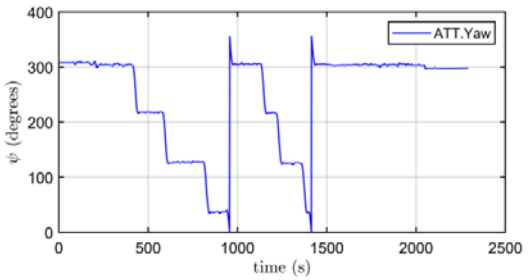

Figure 12: Yaw responses

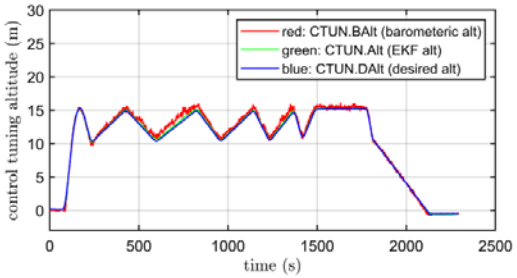

Figure 13: Control tuning altitude

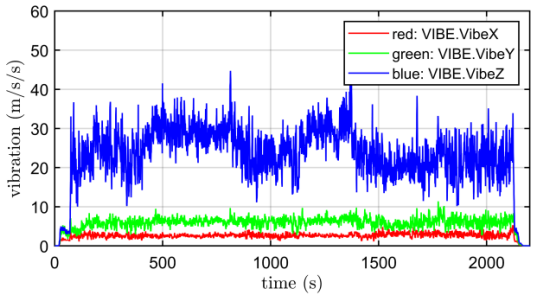

Figure 14: vibrations of X, Y, and Z directions

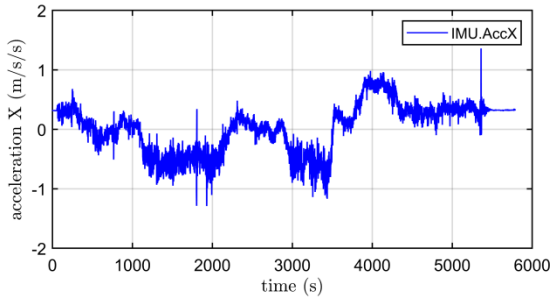

Figure 15: acceleration of X

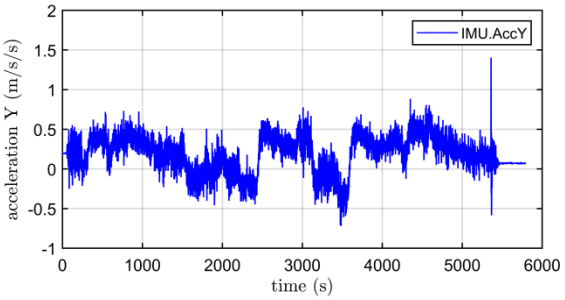

Figure 16: acceleration of Y

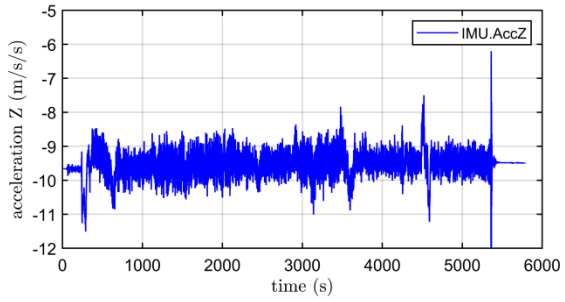

Figure 17: acceleration of Z

During the process of changing the altitude, vibrations along the Z-axis were more dominant. However, we conclude that the experiment demonstrated a safe level of vibration. The vibrations in the X-, Y-, and Z-axes directions are less than 30 m/s/s, which is approved by the UAV flight. The vibrations along the X- and Y-axes were less than 10 m/s/s. (**Figure 14**).

The EKF combines data from rate gyroscope, accelerometer, compass, GPS, airspeed, and barometric pressure measurements **[23]**. The accelerations (X, Y, Z) of the drone are shown in **Figures 15-17**. The Inertial Measurement Unit (IMU) angular rates were converted into angular positions. The accelerations were converted into velocities and positions by integration. Such a process is regarded as 'state prediction' in the EKF system. However, there was a difference between the actual GPS position and the predicted values. This is called 'innovation,' which represents the difference between actual and expected measurements **[33]**.

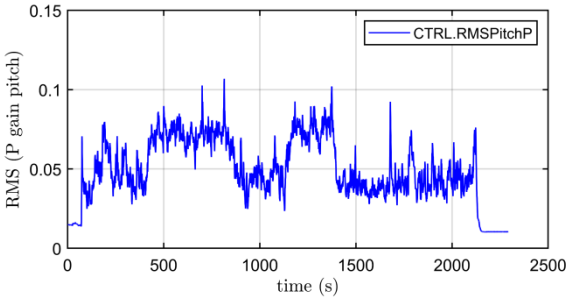

Figure 18: RMS of P gain of pitch

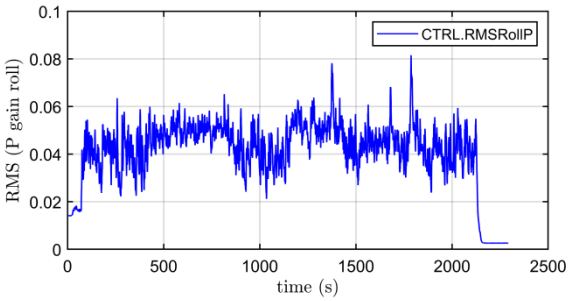

Figure 19: RMS of P gain of roll

Because the KF eliminates the superfluous and cumulative errors in the measurements, it can be considered the recursive solution of the Gauss idea of 'least-squares' **[32]**.

Finally, only the P gain of the PID controller is illustrated in **Figures 18** and **19**. There are two controllers: rate and attitude. There are translational and rotational controllers of drones. Both controllers should be connected in one direction to avoid 'singularity'. However, this study does not address the content of numerical simulations. A PID was adopted as the rate (velocity) controller. For example, the state error between the measured and demanded rates, which are converted in ArduPilot, is multiplied by the P gain. In this case, the root-mean-squared (RMS) P gain was multiplied by the pitch and roll. The RMS estimate of the controller state was updated at each time step.

4. Conclusion

Operating an aerial robot in the field offers a fresh perspective, which is appealing to UAV enthusiasts. However, when applied to marine environments, the size, design, and performance should be carefully considered because the weather conditions of the sea are often harsh. Although drones are attractive to researchers and the public because of their simple structures, low cost, and portable features, the control of UAVs is difficult because their motion characteristics are unique compared to those of surface, ground, and underwater vehicles.

In this study, a hexacopter was constructed for autonomous missions from the ground to merchant ship decks. If drones have inaccurate altitude and position performances in calm weather, how can they fly during bad weather? We then tested autonomous tracking missions based on the ArduPilot program. This is a typical test for UAVs and other autonomous ship models. Guidance laws have been demonstrated for drone-tracking missions. The PID controllers fit well with auto-tuning. The control tuning of altitudes demonstrates that Micro Air Vehicle Link (MAVLink) communication, such as sending commands between the PC and hexacopter, is achieved successfully.

The tracking, driving, vibration, and hovering performances were satisfactory. However, this study has the limitation of a lack of position bias and control techniques. In addition, when the drone was turned at every waypoint, stiff movements and unsmooth attitudes were observed in the physical environment. Thus, smoothing will be necessary in future experiments to reduce abrupt changes. We must improve the hexacopter system and study the concept of 'smoothers' **[32][33]**. The authors concluded that this test is more appropriate for autonomous vehicle tests than numerical studies.

Author Contributions

Conceptualization, S.D. Lee; Methodology, D.J. Kim; Software, K.S. Jang; Validation, C. G. Park; Formal Analysis, S.D. Lee; Investigation, D.J. Kim; Resources, K.S. Jang; Writing—Original Draft Preparation, D.J. Kim; Writing—Review & Editing, S.D. Lee.

References

[1] Flyer, Skyports to launch Royal Mail drone deliveries on Orkney, 2023. https://flyer.co.uk/skyports-to-launch-royal-mail-drone-deliveries-on-orkney/, Accessed August 2, 2025.

[2] Skyports, Royal Mail and Skyports partner on drone delivery, 2020. https://skyportsdroneservices.com/2020/12/royal-mail-and-skyports-partner-on-drone-delivery/, Accessed August 2, 2025.

[3] Marine Technology, Skyports Trials Drone Deliveries for UAV-Enabled Maritime Services, 2025. https://www.marinetechnologynews.com/news/skyports-trials-drone-deliveries-648995, Accessed August 2, 2025.

[4] KEIT (Korea Planning & Evaluation Institute of Industrial Technology), New technology of the Month, pp. 14-15, 2018.

[5] KIAST (Korea Institute of Aviation Safety Technology), Future aviation – export support type, 2022. https://www.kiast.or.kr/kr/sub06_01_14_01.do, Accessed August 2, 2025.

[6] Didiok Makings, TY-3R Waters Emergency Rescue Drone Flying Life Buoy, 2023. https://didiokmaking.com/products/water-rescue-drone-ty-3r-flying-life-buoy?srsltid=AfmBOoom8AQFf0ykIVbmHQBsG33p-KKjLwObrjT1MD72GC7PsV5H9grA, Accessed August 2, 2025.

[7] New Atlas, Hybrid rescue drone flies out to swimmers and becomes a lifebuoy, 2024. https://newatlas.com/drones/ty-3r-flying-lifebouy-drone/, Accessed August 2, 2025.

[8] KBS news, World's First Marine Life Saving with Drones, 2018. https://n.news.naver.com/mnews/article/056/0010538037, Accessed August 2, 2025 (in Korean).

[9] BBC, Drone mail service suspended after device sinks, 2023. https://www.bbc.com/news/articles/c0j29yy4yp3o, Accessed August 2, 2025.

[10] KOPRI (Korea Polar Research Institute), A Planning and preliminary studies for advanced and stable operation on unmanned monitoring in the Antarctica, pp. 24-25, 2015.

[11] WINDRACERS, Windracers ULTRA: Delivering your mission, Windracers Ltd, 2025. https://windracers.com/, Accessed August 2, 2025.

[12] D. K. Le and T. K. Nam, "A study on the modeling of a hexacopter," Journal of Advanced Marine Engineering and Technology, vol. 39, no. 10, pp. 1023-1030, 2015.

[13] ARDUPILOT Versatile, Trusted, Open, ArduPilot Dev Team, 2024. https://ardupilot.org/, Accessed August 2, 2025.

[14] D. Aláez, P. Lopez-Iturri, M. Celaya-Echarri, L. Azpilicueta, F. Falcone, J. Villadangos, and J. J. Astrain, "Digital twin modeling of open category UAV radio communications: A case study," Computer Networks, vol. 242, 110276, 2024.

[15] M. W. Ahmad and M. U. Akram, "UAV sensor failures dataset: Biomisa arducopter sensory critique (BASiC)," Data in Brief, vol. 52, 110069, 2024.

[16] W. Suparta, A. Basuki, and M. Arsyad, "The development of quadcopter using Arducopter APM 2.8 with autopilot for tracking point of drop-off goods", IOP Conference 2023,

Ser.: Earth Environmental Science, vol. 1151, 012032, 2022.

[17] G. R. Bhat, M.A. Dudhedia, R.A. Panchal, Y.S. Shirke, N.R. Angane, S.R. Khonde, S.P. Khedkar, J.R. Pansare, S.S. Bere, R.M. Wahul, S. H. Gawande, "Autonomous drones and their influence on standardization of rules and regulations for operating–A brief overview", Results in Control and Optimization, vol. 14, 100401, 2024.

[18] M. S. Grewal and A. P. Andrews, "Applications of Kalman filtering in aerospace 1960 to the present," IEEE Control Systems Magazine, vol. 30, no. 3, pp. 69-78, 2010.

[19] ARDUPILOT, Connect ESCs and Motors, ArduPilot Dev Team, 2024.

[20] G. V. Raffo, M. G. Ortega, and F. R. Rubio, "An integral predictive/nonlinear $\mathscr{H}\infty$ control structure for a quadrotor helicopter," Automatica, vol. 46, no. 1, pp. 29–39, 2010.

[21] T. Luukkonen, "Modelling and control of quadcopter," Independent research project in applied mathematics, Aalto University, School of Science, 2011.

[22] ARDUPILOT, System ID Mode Operation, Copter documentation, ArduPilot Dev Team, 2024.

[23] ARDUPILOT, Extended Kalman Filter Navigation Overview and Tuning, ArduPilot Dev Team, 2024.

[24] Y. W. Law, Adavanced control, Kalman filter, EEET 4071 Lecture note.

[25] A. Gelb, Applied Optimal Estimation, The M.I.T. press, 1974.

[26] S. J. Chon, J. H. Kim, and J. K. Choi, "Compensated Kalman filter for state estimation of maneuvering target," Journal of Advanced Marine Engineering and Technology, vol. 42, no. 1, pp. 41-48, 2018.

[27] K. Ogata, Modern control engineering, 5th Edition, New Jersey, Pearson, August 25, pp. 31–724, 2009.

[28] WIKIPEDIA, Kalman filter, Wikimedia Foundation, Inc., 2025, https://en.wikipedia.org/wiki/Kalman_filter, Accessed August 2, 2025.

[29] WIKIPEDIA, Extended Kalman filter, Wikimedia Foundation, Inc., 2025, https://en.wikipedia.org/wiki/Extended_Kalman_filter, Accessed August 2, 2025.

[30] G. Welch and G. Bishop, "An introduction to the Kalman Filter, Technical Report", University of North Carolina at Chapel Hill, Chapel Hill, NC, United States, pp. 1-16, 1995.

[31] Y. G. Kim and H. C. Bang, Introduction to Kalman Filter and Its Applications, IntechOpen, pp.1-15, 2018.

[32] A. Gelb, Applied Optimal Estimation, The M.I.T press, 1974.

[33] M. S. Grewal and A. P. Andrews, Kalman Filtering, Theory and Practice using Matlab, 3rd Edition, A John Wiley & Sons, Inc., pp. 51-52, 2008.

[34] ARDUPILOT, Mission Planner Overview, ArduPilot Dev Team, 2024.

[35] WIKIPEDIA, Proportional integral derivative controller, Wikimedia Foundation, Inc., https://en.wikipedia.org/wiki/Proportional%E2%80%93integral%E2%80%93derivative_controller, Accessed August 2, 2025.

[36] ARDUPILOT, Advanced Tuning, ArduPilot Dev Team, 2024.

[37] ARDUPILOT, Manual Tuning of Roll and Pitch, ArduPilot Dev Team, 2024.

[38] S. H. Park, J. Deyst, and J. P. How, "A new nonlinear guidance logic for trajectory tracking," Proceedings of the AIAA Guidance, Navigation and Control Conference, Aug 2004. AIAA-2004-4900, 2004.

[39] S. H. Park, J. Deyst, and J. P. How, "Performance and Lyapunov stability of a nonlinear path-following guidance method," Journal of guidance, control, and dynamics, vol. 30, no. 6, pp. 1718-1728, 2007.

[40] M. Niculescu, "Lateral track control law for aerosonde UAV", 33rd AIAA Aerospace Sciences Meeting and Exhibit, (AIAA 2001-0016), 2001.

[41] E. Kreyszig, Advanced Engineering Mathematics, 10th Edition, A John Wiley & Sons, Inc., 2011.

[42] ARDUPILOT, Understanding Altitude in ArduPilot, ArduPilot Dev Team, 2024.